Visual Saliency based Bas-relief Generation with Symmetry Composition Rule

Tingting Li[1], Liying Yang[1], Meili Wang[1,2,3], Yuling Fan[1,2], Feiyu Zhang[1], Shihui Guo[4], Jian Chang[5], Jian Jun Zhang[5]

[1]College of Information Engineering, Northwest Agriculture and Forestry University, Yangling, Xianyang, China

[2]Key Laboratory of Agricultural Internet of Things, Ministry of Agriculture, Yangling, Xianyang, China

[3]Shaanxi Key Laboratory of Agricultural Information Perception and Intelligent Service, Yangling, Xianyang, China

[4]Software School, Xiamen University, Xiamen, China

[5]National Centre for Computer Animation, Bournemouth University, Bournemouth, UK

Correspondence

Meili Wang, College of Information Engineering, Northwest Agriculture and Forestry University, Yangling, Xianyang, China

Abstract

This paper presents a novel approach for bas-relief generation and synthesis. In contrast to previous methods, we divide this problem into two parts, the selection of the best view and arrangement of the relief layout. Taking these into account, we incorporate the visual saliency and photographic composition rules into the bas-relief generation. Additionally, a nonlinear compression function is used to compress the models. And finally we implement surface parameterization by directly manipulating the mesh triangles to generate curved surface bas-relief. We validate our approach through a variety of models. The results indicate that the proposed approach is effective to adapt different types of target surface with topology unchanged. Comparing to conventional methods, our approach is able to effectively produce bas-relief with reasonable layout and distinct details.

KEYBORDS

bas-relief, visual saliency, symmetry composition

1 INTRODUCTION

Bas-relief is a sculpting art, which carves out the undulation change of a sculpture in a very narrow depth range. The spatial structure of the bas-relief not only shows the three-dimensional (3D) shape, but also has a certain plane modality. As a form of sculpture art, bas-relief can exist as an independent object, or be attached to a surface as well. Furthermore, it can well express the advantages of painting in terms of composition, narration, and theme, which makes the design and production of bas-relief more complicated.

The production techniques used for relief rely on artificial and manual design. The traditional production method is inefficient, which also has a long production cycle and cannot be modified freely. However, recent advances in digital relief generation such as 3D modeling simplify the production of bas-relief. These technologies enable bas-relief to be built in an easy way.

3D digital bas-relief generation algorithms can be divided into two categories: 2D image based[1] and 3D model based[2]. Since a 2D image does not have exact depth information, the general method is converting it to depth image or intensity image. This process usually uses techniques such as image segmentation and 3D model reconstruction to generate bas-relief. The other method is to generate bas-relief based on the 3D model. Select a projection direction that reflects the model features and map the model on a plane or a surface to generate the bas-relief. From the geometric representation, this type of relief generation method can be regarded as a complicated surface that attaches 3D models

Select a projection direction that reflects the model features and map the model on a plane or a surface to generate the bas-relief. From the geometric representation, this type of relief generation method can be regarded as a complicated surface that attaches 3D models to a flat or curved background.

Recently proposed bas-relief generation techniques have become more mature in terms of algorithm adaptability and relief effect [1-4]. However, they do not consider the bas-relief layout, which limits the aesthetic value of their results. The approach in this paper endeavor to address this challenges. The fundamental contributions of our research are as follows.

Arrangement layout. In photography, how to arrange the elements of the picture is already a relatively mature topic. However, they have not applied the relevant principles to the relief layout. We use the symmetry composition rule to arrange the elements of relief.

Attributes of views. To highlight the designers intent, we need to select the best projection direction of the source model. The best view selection involves computing the attributes of views of the 3D mesh model. We propose an approach to calculate the attributes of views by directly manipulating the mesh triangles.

Bas-relief generation. When the source 3D model is attached to the background, the source model will be deformed and lose detail information. Different from the previous algorithms, we take this complex problem to a simple geometric question. Surface parameterization is implemented to attach the 3D model to the background with less deformation.

This paper is organized as follows. Section 2 recalls related works on rules of symmetry composition, measuring view goodness and bas-relief generation. Section 3 details the proposed method. Section 4 conducts experiments and analyze the results. Finally, we conclude in Section 5.

2 Related Work

2.1 Rules of Symmetry Composition

Aesthetics has been a subject of long-standing debates by philosophers and psychologists alike [3]. Relief generation algorithms regularly face the problem of how to compose relief in aesthetically pleasing ways within the mapping range of target object. In the field of art and photography, aesthetics refers to the study of principles that underlie the appreciation of beauty [4]. Advances in the technologies of computer vision have enable us generate artwork more in line with peoples aesthetics. The earliest explicit theory of aesthetics can be found in the writings of Plato [4], who discussed the way in which the parts fitted together, especially their order and structure, which resulted the composition of a speech. Many important characteristics emerged from this principle. First and foremost, small alterations to an entity that is viewed in aesthetic terms, can make very large differences to the aesthetic experience, to the beauty of the entity [5].

Two concepts in the modern literature bear special mention because of their general importance and specific relevance to the research reported on spatial composition: balance and fluency. Balance is one of the most often discussed principles of spatial composition in art [6].

Alexander [6] regarded balance as one of the bases of the aesthetic concept. In his theory, centers are the building blocks of wholeness, and he gave examples to prove the point of view. Gardner [5] performed a user-based research to confirm that people tended to prefer a picture which the objects were positioned along a horizontal axis. The results of their experiments affirm the power of the center and facing direction in the aesthetic biases viewers bring to their appreciation of framed works of visual art [6]. Brachmann and Redies [7] conducted two experiments to investigate the effects of symmetry and balance on the aesthetic appeal of text-overlaid images. And the results showed that subjects are adept at judging radial symmetry about the center point of an image.

2.2 Measuring View Goodness

Observing 3D models from different views reflects different shapes, and reveals different information. For some views people have strong lateralization and orientation bias [8]. How to measure the preference of these views plays a pivotal role in 3D shape analysis. An important aspect of a geometric shape is its saliency, which

are the features that are more pronounced or significant especially when comparing regions of the shape relative to their neighbors [9].

Palmer [10] introdeced the concept of canonical views. Based on their works, Tao et al. [11] presented two structure aware view descriptors to select the optimal viewpoint with the maximum amount of the structural information. Inspired by Shannons information theory, Lee et al. [12] introduced the notion of 3D mesh saliency and called it mesh saliency. The ideas of silhouette stability, object symmetries and shape curvature had also been explored in previous work. Secord et al. [13] combined attributes that measures the attributes of views based on human preference data. Moreover, their work contributed a set of simple recommended measures for practical applications. We use Secord et al' [13] method to select the best view of our source models.

2.3 Bas-relief Generation based on 3D Model

Generation of digital bas-relief based on 3D mesh model was first proposed by Cignoni et al. [14]. They applied a forthright linear compression of the height field to generate bas-relief. However, their method results in a serious loss of the salient shape features of the model. Recently, considerable attention has been paid to preserving visually important details [2].

Song et al. [15] used high dynamic range image compression technology in 3D to emphasize the details. Sun et al. [16] generated digital reliefs by directly processing the height fields of the 3D model, and used histogram equalization to preserve model detail. Liu et al. [17] established a relationship between the source relief and the target area, and designed an algorithm based on normal vector adjustment for relief wrapping on the new base with less distortion. Wang et al. [18] combined the outline of 3D model, render graph and depth map to generate relief. In their next work [19], they proposed a method to generate reliefs using saliency information, and adopted a Poisson equations to boosting of details. Li et al. [20] used the bilateral filter technique and the differential property of Fourier transform to generate relief with preserved detail. The calculation process is completed in the Fourier transform domain. Wang et al. [21] used 3D unsharp masking to enhance the visual features in the 3D mesh, and employed a nonlinear variable scaling scheme to generate the final bas-reliefs. The effectiveness of method has been verified by 3D models printers. The above methods put particular emphasis on detail preservation and compression ratio. Mousa et al. [22] presented spherical harmonics decomposition for spherical functions defining 3D triangulated objects, which applicable for local surface smoothing and interactive geometric texture transfer. Zhou et al. [23] developed an interactive modeling system for complex geometric detail transformation based on an empirical model decomposition of multi-scale 3D shapes. Their method preserved target details into the overall shape of target model, while the source model details can also be interfered by target model. Zhang et al. [24] reconstructed an input object as a continuous relief depth map, and used mesh intersection to paste the relief on the goal object. In contrast to their method, we do not require the model to be converted into depth maps, and the processes are more concise.

3 Our Methods

We propose a bas-relief synthesis technique that is significantly different from the previous methods. In our method, we define the surface which the relief attached on as the target object, and assign the mapping range on the target object and automatically arrange the source model. Then, we compute the attributes of views to select the best view of the source model through linear models of goodness. After that, we use the spatial weight matrix and Laplace operator to enhance details of the model, and use the nonlinear compression to compress the extent of height field, which allows meanwhile suppressing large amplitude regions and enhancing the small amplitude regions. This optimized method of detail preservation increases vividness of the bas-relief. Finally, we adopt surface parameterization to paste the source model onto the target surface. Curved surface bas-relief is therefore generated. Figure 1 illustrates the procedure of our bas-relief generation method.

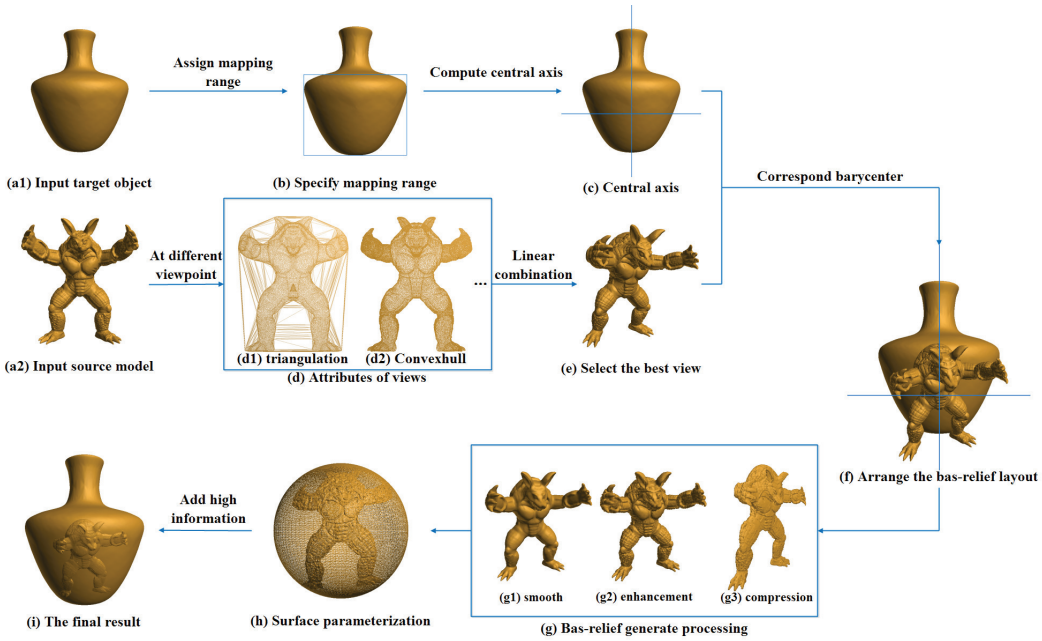

Figure 1: Illustration of our bas-relief generation method.

3.1 *Relief Layout Based on Symmetry Composition Rules*

Our work starts from specifying the mapping range on the target object as the range of relief layout. Then we compute the barycenter of the source model by corresponding it with the center of the mapping range to automatically arrange the source model.

The formula for calculating the models barycenter coordinates is defined by

$$mI = \sum_{i}^{N} \frac{v_i * \sum_j^m S_j}{m} \Big/ N \,, \qquad (1)$$

where v_i denotes the vertex coordinates of the i-th vertex in the 3D source model, m is the number of adjacent mesh triangles of v_i, j is the j-th adjacent mesh triangle of v_i, S_j is the sum area of adjacent mesh triangles of v_i, N is the number of vertices in the 3D model.

We move the source model to the center of the range mapping by using the following equations

$$\begin{aligned} v(x)_1 &= v(x)_1 + \Big(v(x)^B_{min} + \tfrac{1}{2} * \\ &\quad \Big(v(x)^B_{max} - v(x)^B_{min}\Big) - mI_1(x)\Big) \,, \\ v(y)_1 &= v(y)_1 + \Big(v(y)^B_{min} + \tfrac{1}{2} * \\ &\quad \Big(v(y)^B_{max} - v(y)^B_{min}\Big) - mI_1(y)\Big) \,, \end{aligned} \qquad (2)$$

where $v(x)_1$ and $v(y)_1$ denote the x-axis and y-axis coordinates, respectively, of the 3D model, $v(x)^B_{max}$ and $v(x)^B_{min}$ denote the maximum and minimum coordinates, respectively, of the mapping area in the x-axis direction, $v(y)^B_{max}$ and $v(y)^B_{min}$ denote the maximum and minimum coordinates, respectively, of the mapping area in the y-axis direction. Further, $mI_1(x)$ and $mI_1(y)$ are the x-axis and y-axis coordinates, respectively, of barycenter of the model. Figure 2 shows the target objects, and the intersection of the blue lines represents the center of the mapping ranges.

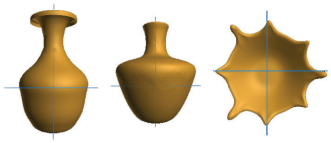

Figure 2: The barycenter of different carriers.

3.2 *Best Viewpoint Selection*

To select the best view of the 3D model, the general way is to use discrete sampling from the view sphere as viewpoints. Secord et al. [13] described a set of view-dependent attributes and evaluated the relative contributions of the different attributes by presenting a large user study and fitting models of viewpoint preference. We present a method to calculate the attributes of

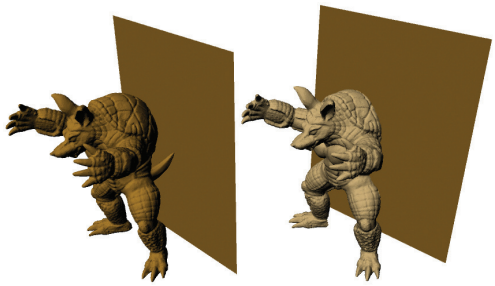

Figure 3: (a) Original object (b) source mesh.

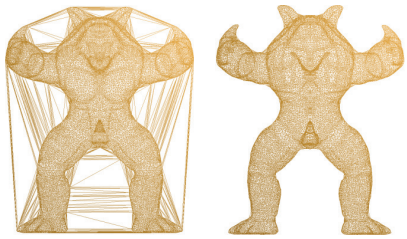

(a) (b)

Figure 4: Delaunay triangulation (a) and its corresponding concave hull (b).

views of 3D mesh model and calculate the visual saliency of the source model referencing [13].

3.2.1 Attributes of Views

This method can directly acquire the projection area and projection contour length without transforming to depth buffer.

First, when we observe a model from a viewpoint direction, some mesh triangles are invisible. Since in the pre-processing step, we reconstruct the source model to remove the useless invisible and blocked mesh triangles. Figure 3 shows the original and the resulting meshes.

Next, we calculate the longest edge length R of all mesh triangles, and eliminate the height information of the vertices, that is, convert a 2.5D model to a planar point set, which recorded as S. While we build the Delaunay triangulation of the point set S^d. The result of this step is shown in Figure 4(a).

At last, we compute the length of the triangle edges of S^d, and the number of the adjacent triangles of each edge. We define the edge adjacent to two triangles as the inner edge, the edge adjacent to one triangle as the boundary, and the edge without an adjacent triangle as the edges degenerated in the calculation process. Furthermore, we construct the concave hull of the points set. The example of the concave hull is shown in Figure 4(b).

The area of the concave hull is the projected area of the 3D model at this view, which equals to the summed area of the triangle of concave hull. Moreover, the edge length of the boundary edges of the concave hull is the projected contour of the model.

3.2.2 Modeling Viewpoint Preferences

The natural extension to the single-attribute models are the linear-K models, which combine K attributes to form a goodness value. We have implemented two linear-K models to select the best view of the 3D models. The general expression for the linear-K model is defined by

$$G(v) = \sum_{j \in S} w_j a_j, \tag{3}$$

where v is the viewpoint, S is the set of indices of attributes used in the particular model ($|S| = K$). At the same viewpoint, for different mathematical models, the score of the viewpoint can be obtained according to the corresponding weight value w_j and known attributes a_j of the views; thus, the best view of the 3D model can be acquired. The weights of viewpoint attributes for different models of viewpoint goodness are shown in Table 1.

Table 1: Weights of viewpoint attributes for models of viewpoint saliency recommended in [13]

	a_1	a_2	a_4	a_7	a_{12}	a_{13}
Single		23				
Linear-3		18	0.51		2.8	
Linear-5	14	14	0.46	2.5	2.7	
Linear-5b	15	2.6	0.42	13		670

In Table 1, a_1 is the projected area of the model in the image plane as a fraction of the overall image area, a_2 defines the surface visibility as the ratio of visible surface area in a particular view to the total surface area of the object, a_4 is the silhouette length, which is the overall length R of the objects silhouettes in the image plane,

(a) (b) (c)

Figure 5: The best view selection results of the bunny.

a_7 is the max depth of 3D model at that viewpoint, a_{12} favors views with a smooth falloff towards the poles, and a_{13} measures how well the eyes of a model can be seen. We have implemented two models, the Linear-5 and Linear-5b models. The two models are calculated as follows:

$$\begin{aligned} &G_1(v) = 14 * a_1 + 14 * a_2 + 0.46 * a_4 \\ &+2.5 * a_7 + 2.7 * a_{12}, \\ &G_2(v) = 13 * a_1 + 15 * a_2 + 0.42 * a_4 \\ &+2.6 * a_{12} + 670 * a_{13}, \end{aligned} \tag{4}$$

where $G_1(v)$ and $G_2(v)$ are the viewpoint rating criteria of the Linear-5 and Linear-5b models respectively.

We chose different rating criteria for different types of model as [13] suggests. For example, the model with eyes is scored using the Linear-5b model. To demonstrate the best viewpoint of the rabbit model, Figure 5(a) shows the default view of the rabbit model, and Figures 5(b) and 5(c) respectively show the best view selection results of the Linear-5 and the Linear-5b model. It can be seen that the result of Linear-5b is more conform to peoples observation habits.

Figure 6 shows the best view results of various 3D models selected by the linear models of goodness. The first column of Figure 6 is the default view of model and the second column is the best view.

(a) (b)

Figure 6: The best view selection results of Multiple models.

3.3 Bas-relief Generation Algorithm

3.3.1 Detail Enhancement

For a bas-relief expression, the visual perception is enhanced through the subtle rises and falls implied by the detail of the 3D models. To obtain bas-relief with obvious features, we enhance the details of the model through the Laplace operator and the spatial weight.

Spatial Weight. The spatial weight is the matrix of the weight ratio between the vertex of the model and the adjacent elements. The critical boundary variables have two expression values, 0 and 1, and if two variables are neighbors, the corresponding expression value is 1 and vice versa [25]. Moreover, we introduce an overall measure to calculate the interaction of two spatial variables, namely, using spatial weight matrix W, which is defined by

$$W_{ij} = [d_{ij}]^{-T} * [\mu_{ij}]^b , \tag{5}$$

where d_{ij} is the distance between elements i and j, μ_{ij} is the ratio of the border shared by elements i and j to the total border of element i. This process is performed by compute_mesh_weight(V, F) in the toolbox_graph Toolkit[26].

In this function, V represents the vertices coordinate information of the 3D model and is stored in the form of a matrix. F represents the mesh triangles of the 3D model. We can obtain the spatial weight matrix of the 3D model by this function.

Laplace operator. In mathematics, the Laplace operator is a differential operator given by the divergence of the gradient of a function in Euclidean space. As the Laplace operator is widely used in image sharpening, using the discrete Laplace operator to extract the detail information from the 3D model is feasible. Laplace operator L can be defined by

$$L = speye(n) - diag\left(sum\left(W, 2\right)^{-1}\right) W, \quad (6)$$

where W is the spatial weight matrix of the model, n is the row of the W.

We use the spatial weight matrix to perform the smooth process. This process is calculated by the following equations:

$$V_2 = \left(W * \left(W * V^T\right)^T\right), \quad (7)$$

$$V = \begin{pmatrix} x_1 & y_1 & z_1 \\ x_2 & y_2 & z_2 \\ \vdots & \vdots & \vdots \\ x_n & y_n & z_n \end{pmatrix}, \quad (8)$$

where V_2 is the low-frequency domain portion of the 3D model, that is, the smooth model. W is the spatial weight matrix, V is the vertex matrix of the 3D model, and x_i, y_i, and z_i respectively represent the x, y, and z coordinates of the i-th vertex, and V^T is the transposed matrix of V. Further, we use the weight matrix to achieve detail enhancement by

$$V_3 = \left(L * \left(L * \left(L * V^T\right)\right)^T\right) + V, \quad (9)$$

where L is the Laplacian matrix of the mesh model, and V_3 is the high-frequency domain of the 3D model, namely, the mesh model that the detail after detail enhancement.

3.3.2 Nonlinear Compression

Linear compression leads to serious details loss [27]. Directly using the hyperbolic tangent function to compress the height gradient can obtain satisfactory convergence results, but the result lack fidelity at both ends of the gradient field. Hence, we propose a new compression function that satisfies all the conditions that a gradient compression function should meet according to Zhou et al. [23]. In our approach, we compress the extent of the height field by combining linear and the nonlinear functions, which can scale the 3D mesh model efficiently. In this case, the compressed height gradient field of model z can be obtain by

$$z = z_a + z_b, \quad (10)$$

where z_a is the linear compression height field and z_b is the nonlinear compression height field. Further,

$$z = \mu * V_2 + tanh\left(w * V_3\right), \quad (11)$$

where $\mu * V_2$ is the linearly compression part, μ is the linear compression coefficient, $tanh\left(w * V_3\right)$ is the nonlinear compression of hyperbolic tangent function, w is the nonlinear compression coefficient. Figures 7(a)-(d) are the source model, linear-compressed mesh, hyperbolic-tangent compressed mesh, and our function-compressed mesh respectively. These figures show that the compressed mesh obtained by our method retains more detail information than those of two methods. For a more intuitive demonstration our method effectivity, we color the gradient field according to the curvature and show it in Figures 7(e)-(h). In these figures, the red represents the sharply deformations and green represents the subtle deformations. The colors closer to Figure 7(e) are more similar to the original shapes, which means the compression method achieves a better result. As we can see from the legs part in Figure 7(h), our compression method retains more details than the other two functions.

Table 2 compares the curvature of different compression methods. According to every evaluation criterion of curvature, the compressed curvature results generated by our method are minimally disparity from the original model.

3.3.3 Surface Parameterization

In this paper, we regard the relief model as one of surfaces that the 2.5D source model attaches

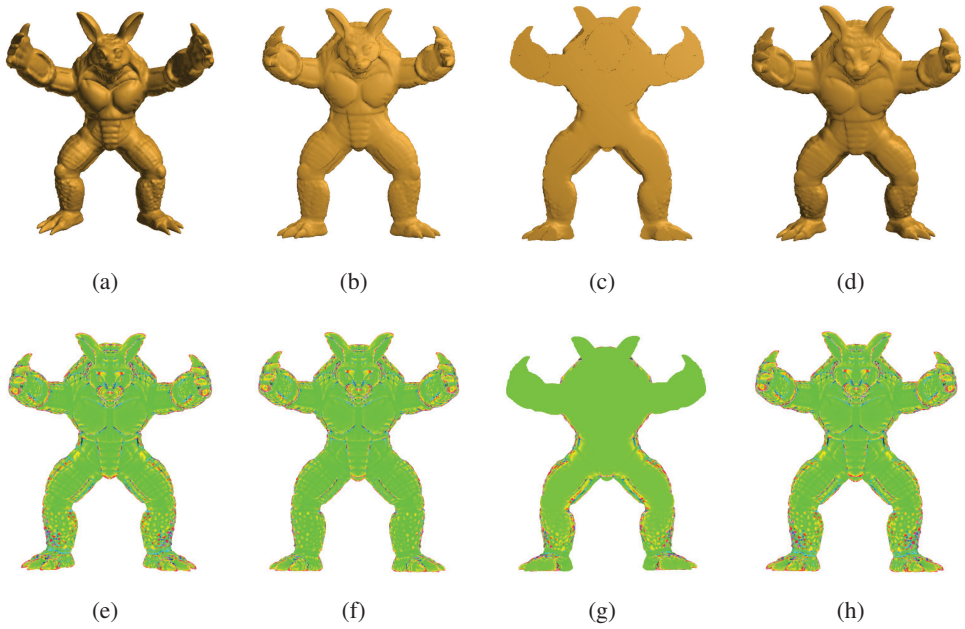

Figure 7: Height field and curvature of the mesh.

Table 2: Different compression methods on the curvature.

Name	Original Model	Linear compression	Hyperbolic tangent compression	Our method
Clip Min	-16.7694	-20.2304	-12.4172	-19.0953
Clip Max	18.5682	22.4491	13.0746	21.2611
Average	0.8994	1.1094	0.3287	1.0829
Varience	5.8896	7.1132	4.2486	6.7261

to a target surface. The mesh triangles of the source model are denotes as B^R and the mesh triangles of the mapping range are denoted as B^T.

First, we remove the height information of B^R and B^T, which are respectively denoted as P^R and P^T. In this case, the vertices' information sets are recorded as S^R and S^T, which are $S^R = \{v_i^R | i = 1, ..., n_1\}$ and $S^T = \{v_i^T | i = 1, ..., n_2\}$, respectively. Figure 8 illustrates this process.

Next, we compute the Euclidean distance between v_i^R and each vertex v_i^T and record the vertex v_j^T with the minimum Euclidean distance, establishing the mapping relationship between v_i^R and v_j^T. We create the mapping set as $S_1 = \{(v_i^R, v_j^T) | min(norm_{i=i_0}(v_{i_0}^R, v_j^T)), v_{i_0}^R \in S^R, v_j^T \in S^T\}$. Figure 9 illustrates this process.

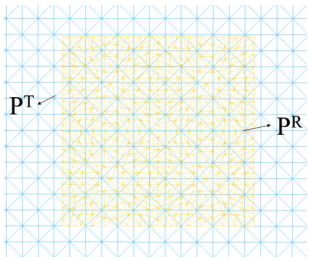

Figure 8: Surface parameterized initialization diagram.

Then, we calculate the mesh triangle of vertex v_i^R that intersects with the adjacent mesh triangles in B^T of the corresponding vertex v_j^T in S_1, compute the intersection coordinates, which are denoted as v_j^{TP}. We record the mapping set $S_2 = \{(v_i^R, v_j^{TP}) | z_i^{TP} = a * x_j^T + b * y_j^T + c * z_j^T - a * x_i^R - b * y_i^R / c\}$. Figure 10 illustrates this process.

Finally, we add the height information to S_2, and reconstruct a 3D model to paste the source model to the target surface.

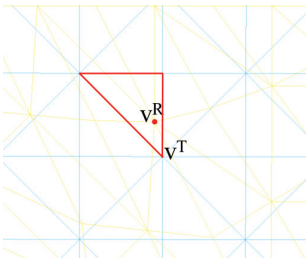

Figure 9: Surface parameterized initialization diagram.

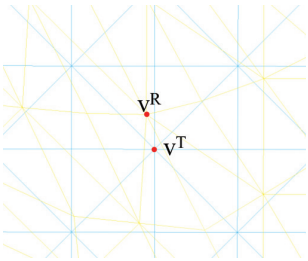

Figure 10: Surface parameterized initialization diagram.

4 Experimental Results and Analysis

To demonstrate the effectiveness of our method, we used six models as input, and mapped the bas-reliefs onto three different target objects. All the experiments were implemented on a PC that has an Inter Core i7-3770 CPU and 8.0GB of RAM using MATLAB 2016a. As shown in Figure 11, the input mesh model has been deformed into the desired form that is attaches to the target objects. The proposed method is applicable to both convex and concave surface in bas-relief generation.

Due to the nature of parametric surfaces, the results of gradient-based mesh deformation will inevitably depend on the mesh triangle shape of the target object. However, the deformation distortion is still under control because the mesh structure conditions have been used to restrict it. As shown in Figure 11, the results in third row have a smoother appearance than the results in the first row, which is attributed to the fact that the third target object has more meshes and the mesh structure is more regular.

In Figure 12, we compare the final results generated from our method and the method in [17]. The comparison shows that, because we enhance the detail, the proposed method retains higher features to create the bas-relief effect. With respect to the process of generation, our method is simpler and does not need subsequent steps such as mesh fusion. Additionally, we attach the relief to a more pragmatic target that provides abundant artistic connotations.

(a) The relief effect generated by the method of

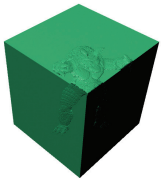

(b) The bas-relief effect generated by our method

Figure 12: Comparison of relief generation effect.

We also compare the relief generation results of our method and those of [20], which uses hyperbolic tangent compression. As shown in Figure 13, our relief has a clearer silhouette benefit from our compression function. The layout of the relief is generated automatically without manual adjustment as well.

(a) The relief effect generated by the method of [25]

(b) The bas-relief effect generated by our method

Figure 13: Comparison of relief generation effect.

Figure 11: Our experiment results.

5 Conclusions and Future Work

In this paper, we introduced a new approach to bas-relief generation and proposed the incorporation of photographic composition principles. Moreover, we added visual saliency to select the best view without user interactions.

Compared with the existing algorithms, our method operates directly on the mesh triangle, which ensures that the mesh topology remains unchanged during geometric processing. The compression function combines linear and nonlinear compression, which enables the bas-relief to reserve more features. Owing to our simple but effective surface parameterization process, the bas-relief is represented in a more flexible manner, which enables us to expand the application scope. By experimenting on a variety of models, the proposed method is able to effectively generate plausible and impressive relief models with layout.

However, there are some limitations of our proposed method, it is only suitable for arranging one model to generate a relief, without considering the influence of the curvature of the target surface on the users cognition. In addition, the generated bas-relief does not have sufficient narrative ability and does not adequately exploit the composition and content of classic painting and photographic works. In the future, we expect to achieve more progress in these aspects.

References

[1] J. Wu, R R. Martin, P L. Rosin, and X. Sun. Making bas-reliefs from photographs of human faces. *Computer-Aided Design*, 45(3):671–682, 2013.

[2] Y. Zhang, C. Zhang, W Wang, and Y. Chen. Adaptive bas-relief generation from 3d object under illumination. In

Computer Graphics Forum, volume 35, pages 311–321. Wiley Online Library, 2016.

[3] A. Brachmann and C. Redies. Computational and experimental approaches to visual aesthetics. *Frontiers in Computational Neuroscience*, 11:102, 2017.

[4] L. Yao. Automated analysis of composition and style of photographs and paintings. *Dissertations & Theses - Gradworks*, 2013.

[5] J S. Gardner. Aesthetics of spatial composition: Facing, position, and context, and the theory of representational fit. *Dissertations & Theses - Gradworks*, 2011.

[6] C. Alexander. The luminous ground: The nature of order: An essay on the art of building and the nature of the universe. *Art Book*, 12(4):58–60, 2004.

[7] A. Brachmann and C. Redies. Computational and experimental approaches to visual aesthetics. *Frontiers in Computational Neuroscience*, 11:102, 2017.

[8] B. Rossion, C A. Joyce, G W. Cottrell, and M J. Tarr. Early lateralization and orientation tuning for face, word, and object processing in the visual cortex. *Neuroimage*, 20(3):1609–1624, 2003.

[9] L. Manfred, K. Dev, W. Shi, D. Julie, and R. Holly. Tactile mesh saliency. *ACM Transactions on Graphics TOG*, 35(4):52, 2016.

[10] S. Palmer. Canonical perspective and the perception of objects. *Attention and performance*, pages 135–151, 1981.

[11] Y. Tao, H. Lin, H. Bao, and F. Dong. Structure-aware viewpoint selection for volume visualization. In *Visualization Symposium, 2009. PacificVis '09. IEEE Pacific*, pages 193–200, 2009.

[12] C H. Lee, A. Varshney, and J. David W. Mesh saliency. In *ACM transactions on graphics (TOG)*, volume 24, pages 659–666. ACM, 2005.

[13] A. Secord, Lu. Jingwan, F. Adam, and S. Manish. Perceptual models of viewpoint preference. *ACM Transactions on Graphics (TOG)*, 30(5):109, 2011.

[14] P. Cignoni, C. Montani, and R. Scopigno. Computer-assisted generation of bas-and high-reliefs. *Journal of graphics tools*, 2(3):15–28, 1997.

[15] W. Song, A. Belyaev, and H P Seidel. Automatic generation of bas-reliefs from 3d shapes. In *IEEE International Conference on Shape Modeling and Applications*, pages 211–214. IEEE, 2007.

[16] X. Sun, P L. Rosin, R R. Martin, and F C. Langbein. Bas-relief generation using adaptive histogram equalization. *IEEE transactions on visualization and computer graphics*, 15(4):642–653, 2009.

[17] S. Liu, T. Zheng, B. Li, and L. Zhang. Relief pasting algorithm based on normal vector adjustment. *Journal of Computer Applications*, 31(1):33–36, 2011.

[18] M. Wang, J. Chang, J. Kerber, and J. Zhang. A framework for digital sunken relief generation based on 3d geometric models. *The Visual Computer*, 28(11):1127–1137, 2012.

[19] M. Wang, S. Guo, H. Zhang, D. He, C. Jian, and J. Zhang. Saliency-based relief generation. *Iete Technical Review*, 30(6):454–480, 2013.

[20] B. Li, S. Liu, and L Zhang. Detail-preserving bas-relief on surface from 3d sceme. *Journal of Computer-Aided Design & Computer Graphics*, 24(6):799–807, 2012.

[21] M. Wang, Y. Sun, H. Zhang, K. Qian, C. Jian, and D. He. Digital relief generation from 3d models. *Chinese Journal of Mechanical Engineering*, 29(6):1128–1133, 2016.

[22] M. Mousa, Raphaelle. C, Akkouche. S, and Eric. G. Efficient spherical harmonics representation of 3d objects. In *Computer Graphics and Applications, 2007. PG*

’07. Pacific Conference on, pages 248–255, 2007.

[23] S. Zhou and L. Liu. Realtime digital bas-relief modeling. Journal of Computer-Aided Design & Computer Graphics, 22(3):434–439, 2010.

[24] D. Zhang, X. Wang, J. Hu, and H. Qin. Interactive modeling of complex geometric details based on empirical mode decomposition for multi-scale 3d shapes. Computer-Aided Design, 87:1–10, 2017.

[25] A. Getis. Spatial autocorrelation: A primer. washington. DC: Association of American Geographers, 1987.

[26] G. Peyre. Graphtheory toolbox. http://cn.mathworks.com/matlabcentral/fileexchange/5355-toolbox-graph/. Accessed 19 Jul, 2016.

[27] Y. Zhang, . Zhou, Y, X. Li, H. Liu, and L. Zhang. Bas-relief generation and shape editing through gradient-based mesh deformation. IEEE transactions on visualization and computer graphics, 21(3):328–338, 2015.

Tingting Li received her B. E. degree in College of Information Engineering from Nort hwest A&F University in 201 6. She is currently pursuing M.E. degree in College of Information Engineering, Northwest A&F University. Her research interests include computer graphics, digital relief generation, and virtual reality.

Liying Yang received her B. E. degree in College of Mathematics and Information Science from Hebei Normal University in 2016. She is currently pursuing M.E. degree in College of Information Engineering, Northwest A&F University. Her research interests include computer graphics, 3D reconstruction, and virtual reality.

Meili Wang is an associate professor at College of Information Engineering, Northwest A&F University. She received her PhD degree in computer animation in 2011 at the National Centre for Computer Animation, Bourne mouth University. Her research interests include computer graphics, geometric modelling, image processing, visualization and virtual reality

Yuling Fan received her B.E. degree in College of Information Engineering from Northwest A&F University in 2015. She is currently pursuing M. E. degree in College of Information Engineering, Northwest A&F University. Her research interests include computer g -raphics, point cloud processin -g, and virtual reality.

Feiyu Zhang is currently purs uing B.E. degree in College o -f Information Engineering, N-orthwest A&F University. His research interests include co-mputer graphics, intelligence a lgorithm, and software enginee -ring.

Shihui Guo is a postdoc-track assistant professor at School of Software, Xiamen Universit y. He received his PhD in co mputer animation from Nation al Centre for Computer Anim ation, Bourne mouth Universit y, UK, and B.S. in Electrical Engineering from Peking Univ ersity, China. His research int erests include character animat ion, 3D printing and robotics.

Jian Chang is Professor at t-he National Centre for Comp-uter Animation, Bournemouth University. He received his P h.D. degree in computer grap-hics in 2007 at the National Centre for Computer Animati-on, Bournemouth University. His research focuses on physi cally-based modelling, motion synthesis, virtual reality, and n -ovel HCI (eye tracking, gest-ure control and haptic).

Jian Jun Zhang is Professor of Computer Graphics at the National Centre for Computer-Animation, Bournemouth Uni -versity. He leads the Comput-er Animation Research Centre. His research interests include computer graphics, computer animation, physically based si-mulation, geometric modelling, medical simulation and visual -ization.